

Molecular Photoacoustic Tomography with Colloidal Nanobeacons**

Dipanjan Pan,* Manojit Pramanik, Angana Senpan, Xinmai Yang, Kwang H. Song, Mike J. Scott, Huiying Zhang, Patrick J. Gaffney, Samuel A. Wickline, Lihong V. Wang,* and Gregory M. Lanza

Molecular imaging has emerged as an interdisciplinary area that shows promise in understanding the components, processes, dynamics, and therapies of a disease at a molecular level.^[1,2] The unprecedented potential of nanoplatforms for early detection, diagnosis, and personalized treatment of diseases is being explored in every noninvasive biomedical imaging method.^[3] Despite myriad advances in the past decade, developing contrast agents with prerequisite features for these imaging modalities continues to remain a challenge.

In the last decade, photoacoustic tomography (PAT) has been of particular interest because of its satisfactory spatial resolution and high soft-tissue contrast.^[4-9] PAT is a novel, hybrid, and nonionizing imaging method that combine the merits of both optical and ultrasonic imaging. It is highly sensitive to the optical absorption of biological tissue. In PAT, tissue is irradiated with a short-pulsed laser beam. Absorption of optical energy causes thermoelastic expansion and radiates photoacoustic (PA) waves from within the irradiated tissue. A wide-band ultrasonic transducer is employed to acquire the PA waves, which are then used to quantify the optical absorption distribution in the tissue. As optical absorption is sensitive to physiological parameters, such as the concentration and oxygenation of hemoglobin, PAT has the potential to provide both functional and molecular imaging *in vivo*. PAT has been used for imaging and quantifying the levels of vascularization and oxygen saturation in tumors.^[4-7] These

features are associated with angiogenesis and hypoxia accompanying malignant tumors.^[10] A number of contrast agents for PAT have been suggested recently,^[5,11] but only a few were shown to have the potential for targeted imaging. To achieve molecular PAT, a major and mostly uninvestigated task is to develop nanometric molecular contrast agents. The prerequisite features include improved properties, such as contrast enhancement, stability, and high target specificity.

We have prepared a novel class of accessible and commercially amenable platform technologies (Figure 1). Colloidal gold nanobeacons (GNBs) of a “soft” nature are used to target vascular pathology, such as thrombus (fibrin),

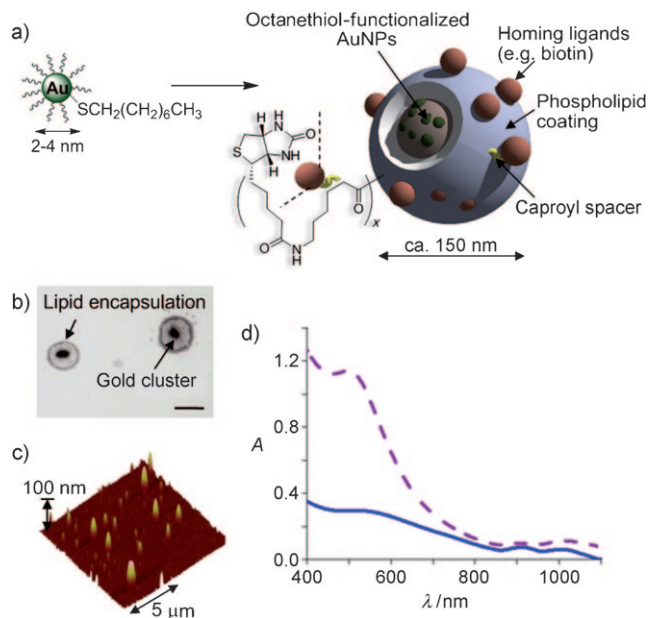


Figure 1. a) Preparation of gold nanobeacons from octanethiol-functionalized gold nanoparticles (AuNPs). $x = 1-2$ mol% phospholipid coating. b) TEM image of gold nanobeacons (drop deposited over nickel grid, 1% uranyl acetate; scale bar: 100 nm). c) AFM image of gold nanobeacons. Average height $H_{av}/nm = (101 \pm 51)$ nm. d) UV/Vis spectroscopic profile. Solid blue line: gold nanobeacons; purple dashed line: octanethiol-coated AuNPs. Spectra are not normalized.

the proximate cause of stroke, and myocardial infarction. Our hypothesis is that GNBs will act as an exogenous contrast agent and could be used as a targeted molecular agent in PAT. In a typical synthesis (Figure 1 a), a commercially available octanethiol-coated gold nanoparticle (AuNP, 2 w/v %, 2–4 nm) that is soluble in organic solvents is suspended in almond oil (20 vol %) and microfluidized with phospholipid

[*] Dr. D. Pan,^[†] Dr. A. Senpan, M. J. Scott, H. Zhang, Prof. S. A. Wickline, Prof. G. M. Lanza
C-TRAIN and Division of Cardiology
Washington University School of Medicine
4320 Forest Park Avenue, Saint Louis, MO 63108 (USA)
Fax: (+1) 314-454-7490
E-mail: dipanjan@wustl.edu

M. Pramanik,^[†] X. Yang, K. H. Song, Prof. L. H. V. Wang
Department of Biomedical Engineering
Washington University in St. Louis
One Brookings Drive, St. Louis, MO 63130 (USA)
Fax: (+1) 314-935-7448
E-mail: lhwang@biomed.wustl.edu

Dr. P. J. Gaffney
Department of Surgery
St Thomas's Hospital, London (UK)

[†] These authors contributed equally to this work.

[**] Financial support from the AHA under grant number 0835426N (D.P.) and from NIH under grant numbers NS059302, CA119342 (G.M.L.), HL073646 (S.A.W.), U54 CA136398, R01EB000712, R01NS046214, and EB008085 (L.V.W.) is greatly appreciated.

Supporting information for this article is available on the WWW under <http://dx.doi.org/10.1002/anie.200805947>.

surfactants (2 vol %). The surfactant mixture is comprised of phosphatidylcholine (lecithin-egg PC, 91 mol% of lipid constituents), cholesterol (8 mol %) and biotin-caproyl-phosphatidylethanolamine (1 mol %). This synthesis resulted in approximately 1200 biotin units per nanoparticle for biotin-avidin interaction. A control nanobeacon was prepared identically except for exclusion of the gold nanoparticles.

The GNB particles have a nominal hydrodynamic diameter of (154 ± 10) nm. The polydispersity and zeta potential were measured to be (0.08 ± 0.03) and (-47 ± 7) mV, respectively. Gold content, determined by ICP-MS, was $1080 \mu\text{g g}^{-1}$ of the 20% colloid suspension. UV/Vis spectroscopy (Figure 1d) showed absorptions at about 520 nm and in the near-IR (NIR) window (ca. 900 nm), which corresponds to the presence of gold nanobecons. The particle size and zeta potential of these nanobecons varied less than 5% over more than 100 days when stored at 4 °C under argon in sealed serum vials (see the Supporting Information). Nanocrystal platforms (< 50 nm) for NIR contrast have been reported;^[5,11] however, particles in this size range rapidly distribute beyond the vasculature and into tissues where binding to non-target cells or simple matrix entrapment can lead to nonspecific signals and increased background noise. For GNBs, the tiny metallic gold nanoparticles (2–4 nm) are incorporated within a larger, vascular-constrained colloidal particle that is constrained to the circulation and intraluminal accessible biomarkers.

Figure 2a shows the PA signals (excitation wavelength $\lambda = 764$ nm) obtained from a tygon tube (inside diameter 250 μm , outside diameter 500 μm) filled with GNBs and whole rat blood. At this excitation wavelength, the peak-to-peak PA

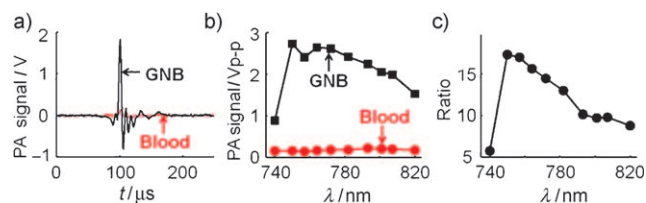


Figure 2. a) PA spectroscopy signals generated from a tygon tube filled with GNBs and rat blood. b) PA spectrum of GNBs and rat blood over a 740–820 nm NIR wavelength range. c) Ratio of the peak-to-peak PA signal amplitudes generated from GNB to those of blood.

signal amplitude V_{p-p} obtained from GNB is about 2.64 V, compared to the circa 0.17 V peak-to-peak PA signal amplitude from rat blood (Figure 2b). Figure 2c shows the ratio of the peak-to-peak PA signal amplitude of GNB to that of rat blood. The PA signal from the tygon tube filled with GNBs is more than 15 times stronger than that from rat blood. Over the 740–820 nm window, the PA signal from GNB is more than ten times stronger. The NIR window is well-known for providing deep tissue PA imaging at the expense of blood contrast owing to the weak blood absorption. The strong PA signal from GNB in the NIR region indicates the potential for molecular PAT of this platform.

The concept of molecular PAT of fibrin, a critical component of intravascular thromboses, was then studied in

vitro. Using acellular fibrin clot phantoms, the biotinylated gold nanobecons and the control nanobecons (that is, containing no metal) were targeted to the fibrin clots with classic avidin–biotin interactions using a well-characterized biotinylated anti-human fibrin-specific monoclonal antibody (NIB5F3).^[12] Figure 3a and b show cross-sectional PAT

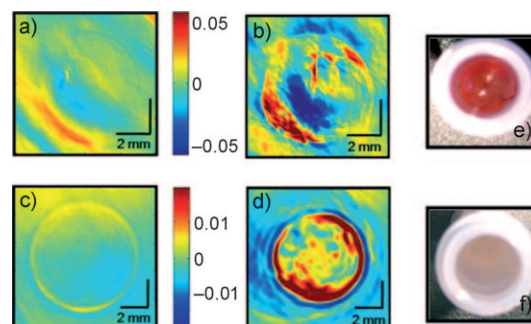


Figure 3. a–d) Cross-sectional PA images of an LDPE tube filled with plasma clot. Color bars between images refer to both images. a) control, b) targeted with GNBs using a curved-array PA system ($\lambda = 800$ nm). c) Control, d) targeted with GNBs using a photoacoustic breast scanner system ($\lambda = 532$ nm). e, f) Optical images of plasma clots stained with Biebrich scarlet acid fuchsin solution: e) targeted with GNB, f) control.

images of a LDPE (low-density polyethylene) tube (ca. 1 cm³ volume, inside diameter ca. 6 mm) filled with plasma clot (control) and plasma clot targeted with biotinylated GNB using a curved array PAT system.^[13] An 800 nm wavelength laser was used for the light source. The control clot treated with targeted nonmetallic nanoparticles has negligible contrast (Figure 3a), whereas the targeted fibrin clot shows up in the PAT image (Figure 3b) with high contrast. Figure 3c and d show cross-sectional PAT images, using a PA breast scanner system,^[14] of the same control and targeted plasma clot. For this system, a 532 nm wavelength laser source was used. As expected, the targeted plasma clot is clearly visible (Figure 3d) in the PAT image, whereas the control image does not show any plasma clot (Figure 3c). We have analytically tested the clot phantoms targeted with three controls for total gold content analyses. The total gold content of the clots targeted with biotinylated GNB (with gold), non-biotinylated GNB (with gold), and biotinylated control nanobecons (no gold), as determined by ICP-MS, were found to be $47 \mu\text{g g}^{-1}$, ND (not detected, $< 0.02 \mu\text{g g}^{-1}$) and ND, respectively. The in vitro images along with ICP-MS data of the targeted plasma clots illustrate the concept of intravascular PAT with GNBs.

Preliminary in vivo blood-vessel imaging was performed non-invasively in a rat model. The pharmacokinetics of GNBs in a blood vessel following intravenous injection (3 mL kg^{-1}) was monitored from femoral vein as changes in the PA signal with time (Figure 4a). As is desirable for molecular imaging, the detection of GNBs as a blood pool contrast agent required a three-fold higher intravenous dose than would routinely be required for targeted imaging. The expected biexponential decay of the PAT signal in blood is similar to reports with other nanoparticles.^[1c] Figure 4b shows a representative

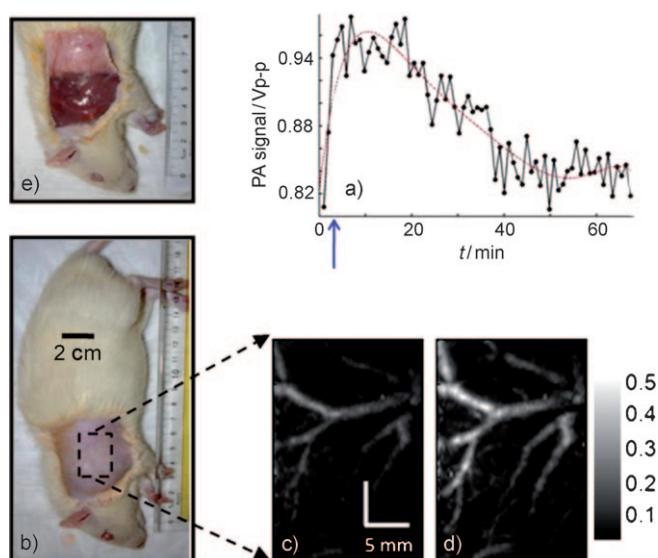


Figure 4. Non-invasive in vivo PA imaging (MAP)^[15] of a rat. For all PA images, the laser was tuned to $\lambda = 766$ nm. a) Pharmacokinetics of GNBs in a blood vessel after injection (point of injection marked by blue arrow). The PA signal from the femoral vein was monitored as an intravenous injection was given with 3 mL kg^{-1} doses through a tail vein. Red curve: sixth-order polynomial fit. b) Photograph of the rat after hair removal from the scanning region before taking the PA images. The scanning region is marked with a black dotted square. c) Control PA image acquired before GNB injection. Bright parts represent optical absorption from blood vessels. d) PA image (MAP) acquired after 156 min of GNB injection. Gray scale bar corresponds to both (c) and (d). e) Optical photograph of the rat with the skin removed after PA imaging.

digital photograph of a rat taken prior to imaging, with the auxiliary surface shaved. Figure 4c shows the maximum amplitude projection (MAP)^[15] photoacoustic image. The vasculature was imaged with a high contrast-to-noise ratio (CNR = 50) and high spatial resolution of about $500 \mu\text{m}$. Photoacoustic images were taken immediately after the GNB injection with an interval of 25–30 min. Figure 4d shows the photoacoustic MAP^[15] image (CNR = 68) of the same area 156 min after the injection (see the Supporting Information for details). As evident from Figure 4d, the signal amplitude of the blood vessels was increased by up to 60% compared to that in the control blood vessels, after 0.075 mL GNB injection.

In summary, we have successfully demonstrated the potential for targeted molecular PAT of gold nanobeacons as exogenous contrast agents. The GNBs provide a more than tenfold signal enhancement in PAT in the NIR wavelength window. The in vitro and preliminary in vivo PAT images both in the NIR wavelength and in the visible wavelength substantiate our hypothesis.

Experimental Section

Preparation of GNBs: In a typical procedure, octanethiol-coated gold nanoparticles (2–4 nm) in toluene (100 mg) are suspended in almond oil (4 mL) and vigorously vortexed to homogeneity. The suspension was filtered through a small bed of cotton. The solvent was

evaporated under reduced pressure at 60°C . The surfactant co-mixture included high-purity egg yolk phosphatidylcholine (91 mol%, 377.4 mg), cholesterol (8 mol%, 16.9 mg), and biotinylated dipalmitoyl phosphatidylethanolamine (1 mol%, 5.8 mg). The surfactant co-mixture was dissolved in chloroform, evaporated under reduced pressure, dried in a vacuum oven at 40°C overnight, and dispersed into water by probe sonication. This suspension was combined with the gold nanoparticles suspended in almond oil (20% v/v, $0.2 \mu\text{M}$) in distilled deionized water (77.3% w/v), and glycerin (1.7% w/v). The mixture was continuously processed thereafter at 20000 psi (ca. 137.9 MPa) for 4 min with an S110 Microfluidics emulsifier at 4°C . The nanobeacons were dialyzed against water using a 20000 Da MWCO cellulose membrane for a prolonged period of time (3 days) and then passed through a $0.45 \mu\text{m}$ Acrodisc syringe filter. To prevent bacterial growth, the nanobeacons were stored under an argon atmosphere (typically at 4°C). Dynamic light scattering: average diameter $D_{\text{av}} = (154 \pm 10) \text{ nm}$; $\zeta = (-47 \pm 7) \text{ mV}$. AFM: average height $H_{\text{av}} = (101 \pm 51) \text{ nm}$. (For details, see the Supporting Information).

Photoacoustic spectroscopy:^[16] Light source: tunable Ti:sapphire laser (LT-2211A, LOTIS TII) pumped by a Q-switched Nd:YAG (LS-2137/2, LOTIS TII); pulse width $< 15 \text{ ns}$, pulse repetition rate 10 Hz. The incident laser fluence on the sample surface was controlled to conform to the American National Standards Institute standards.^[17] Transducer: 5 MHz central frequency, spherically focused, 2.54 cm focus length; 1.91 cm diameter active area element, 72% bandwidth (V308, Panametrics-NDT); low-noise amplifier (5072PR, Panametrics-NDT). Data were acquired with a digital oscilloscope (TDS 5054, Tektronix).

Received: December 5, 2008

Revised: March 6, 2009

Published online: May 5, 2009

Keywords: contrast agents · gold · molecular imaging · nanoparticles · photoacoustic tomography

- [1] a) R. Weissleder, U. Mahmood, *Radiology* **2001**, *219*, 316–333; b) G. M. Whitesides, *Small* **2005**, *1*, 172–179; c) P. M. Winter, S. D. Caruthers, S. A. Wickline, G. M. Lanza, *Nanofabr. Biomed. Appl.* **2005**, 227–249; d) I. J. Majoros, J. R. Baker, Jr., *Dendrimer Based Nanomedicine*, Pan Stanford Pb., Singapore, **2008**; e) D. Pan, S. W. Wickline, G. M. Lanza, S. D. Caruthers, *Eur. J. Radiol.* **2009**, DOI: 10.1016/j.ejrad.2009.01.042.
- [2] a) S. D. Caruthers, S. A. Wickline, G. M. Lanza, *Curr. Opin. Biotechnol.* **2007**, *18*, 26–30; b) R. Weissleder, K. Kelly, E. Y. Sun, T. Shtatland, L. Josephson, *Nat. Biotechnol.* **2005**, *23*, 1418–1423.
- [3] a) C. J. Hawker, K. L. Wooley, *Science* **2005**, *309*, 1200–1205; b) R. K. O'Reilly, C. J. Hawker, K. L. Wooley, *Chem. Soc. Rev.* **2006**, *35*, 1068–1083.
- [4] X. D. Wang, Y. J. Pang, G. Ku, X. Y. Xie, G. Stoica, L. H. V. Wang, *Nat. Biotechnol.* **2003**, *21*, 803–806.
- [5] M. L. Li, J. T. Oh, X. Y. Xie, G. Ku, W. Wang, C. Li, G. Lungu, G. Stoica, L. H. V. Wang, *Proc. IEEE* **2008**, *96*, 481–489.
- [6] X. D. Wang, X. Y. Xie, G. Ku, L. H. V. Wang, *J. Biomed. Opt.* **2006**, *11*, 024015.
- [7] G. F. Lungu, M. L. Li, X. Y. Xie, L. H. V. Wang, G. Stoica, *Int. J. Oncol.* **2007**, *30*, 45–54.
- [8] G. Ku, X. D. Wang, G. Stoica, L. H. V. Wang, *Phys. Med. Biol.* **2004**, *49*, 1329–1338.
- [9] G. Ku, X. D. Wang, X. Y. Xie, G. Stoica, L. H. V. Wang, *Appl. Opt.* **2005**, *44*, 770–775.
- [10] a) B. P. Schneider, K. D. Miller, *J. Clin. Oncol.* **2005**, *23*, 1782–1790; b) P. Vaupel, A. Mayer, S. Briest, M. Hockel, *Oxygen Transp. Tissue XXVI* **2005**, *566*, 333–342.

- [11] a) A. Agarwal, S. W. Huang, M. O'Donnell, K. C. Day, M. Day, N. Kotov, S. Ashkenazi, *J. Appl. Phys.* **2007**, *102*, 064701; b) A. De La Zerda, C. Zavaleta, S. Keren, S. Vaithilingam, S. Bodapati, Z. Liu, J. Levi, B. R. Smith, T.-J. Ma, O. Oralkan, Z. Cheng, X. Chen, H. Dai, B. T. Khuri-Yakub, S. S. Gambhir, *Nat. Nanotechnol.* **2008**, *3*, 557–562.
- [12] S. Raut, P. J. Gaffney, *Thromb. Haemostasis* **1996**, *76*, 56–64.
- [13] K. H. Song, L. H. V. Wang, *J. Biomed. Opt.* **2007**, *12*, 060503.
- [14] M. Pramanik, G. Ku, C. H. Li, L. H. V. Wang, *Med. Phys.* **2008**, *35*, 2218–2223.
- [15] H. F. Zhang, K. Maslov, G. Stoica, L. H. V. Wang, *Nat. Biotechnol.* **2006**, *24*, 848–851.
- [16] K. H. Song, L. H. V. Wang, *J. Biomed. Opt.* **2007**, *12*, 060503.
- [17] Laser Institute of America, American National Standard for Safe Use of Lasers ANSI Z136.1–2000, American National Standards Institute, New York, NY, **2000**.
-